

# Local Learning Rules for Out-of-Equilibrium Physical Generative Models

Cyrill Bösch,<sup>1,\*</sup> Geoffrey Roeder,<sup>1</sup> Marc Serra-Garcia,<sup>2</sup> and Ryan P. Adams<sup>1</sup>

<sup>1</sup>*Department of Computer Science, Princeton University, Princeton, NJ 08540, USA*

<sup>2</sup>*AMOLF, Science Park 104, 1098 XG Amsterdam, The Netherlands*

(Dated: August 27, 2025)

We show that the out-of-equilibrium driving protocol of score-based generative models (SGMs) can be learned via local learning rules. The gradient with respect to the parameters of the driving protocol is computed directly from force measurements or from observed system dynamics. As a demonstration, we implement an SGM in a network of driven, nonlinear, overdamped oscillators coupled to a thermal bath. We first apply it to the problem of sampling from a mixture of two Gaussians in 2D. Finally, we train a  $12 \times 12$  oscillator network on the MNIST dataset to generate images of handwritten digits “0” and “1”.

*Introduction*—Physical systems follow complex, stochastic evolution laws, and thus can be seen as special-purpose computers. This paradigm of computation—sometimes referred to as physical computing—has seen a renaissance in recent years [1–14]. While such physical computers are typically designed by solving global optimization problems, the brain works by forming connections based on local information [15–17]. Physical learning seeks to mimic this learning process in synthetic materials [18–23]. This has been successfully implemented in resistor networks [24, 25], Ising Machines [26, 27] and physical instantiations of Boltzmann machines [28–30] among others [31]. However, such learning rules typically rely on the notion of an equilibrium or steady state of the system dynamics [19, 21, 32]. In this Letter, we demonstrate learning in diffusion-based generative models that fundamentally rely on being out-of-equilibrium. We introduce “force matching”, a local learning rule derived from score matching (SM) [33]—the algorithm underlying score-based generative models (SGMs) [34]. Second, we discuss how a variant of contrastive divergence can be used instead, if such force measurements are not accessible. In contrast to force matching, this approach requires characterization of physical time scales and high time-resolution observations with respect to those time scales. We then numerically train a network of oscillators to implement a generative model—learning the time-dependent, out-of-equilibrium driving protocol required for the system to sample from a target distribution.

Generative modeling is the task of learning to draw samples from a distribution  $p$ . Typically,  $p$  is not available in closed form; instead, we have access to it only through a dataset of  $M$  samples,  $\mathcal{D} = \{\mathbf{x}^{(m)} \in \mathbb{R}^N\}_{m=1}^M$ . It poses a fundamental problem in machine learning and statistics, with applications ranging from image generation [35–37] to the discovery of novel proteins [38]. Traditional approaches based on equilibrium sampling (ES), such as Boltzmann machines [39–41], demon-

strated that physical systems can be harnessed to sample from complex distributions through stochastic relaxation. However, equilibrium methods typically suffer from long and unpredictable convergence times, as tunneling between isolated high-probability regions is exponentially unlikely [42]. Moreover, such Markov processes often traverse low-probability regions, where learned models are less reliable due to data scarcity [34]. A promising alternative lies in non-equilibrium processes, where a simple, typically Gaussian distribution is evolved into the target distribution within finite time [35, 43, 44]. These approaches can improve sampling efficiency and make better use of training data by avoiding extended exploration of poorly modeled regions. Among the most successful methods are score-based generative models (SGMs), which generate samples by solving non-equilibrium stochastic differential equations (SDEs) [34, 35].

SGMs frame generation as the process of denoising a sample of pure noise. A “forward” process is designed to add noise to the data and then a “reverse” process is learned for removing the noise; this yields a generative model. Adding noise to the samples of  $\mathcal{D}$  is done via a linear SDE [35]. Here we pick [36]:

$$d\mathbf{x} = -\mathbf{x} dt + \sqrt{2k_B T} d\mathbf{w}, \quad \mathbf{x} \in \mathbb{R}^N, t \in [0, \tau] \quad (1)$$

where  $d\mathbf{w}$  denotes a Wiener process,  $k_B$  is the Boltzmann constant and  $T$  is the temperature of the thermal bath. We assume that the associated probability flow  $p_t$ , with  $p_0 = p$ , converges sufficiently well to  $p_\tau \approx \mathcal{N}(0, k_B T \mathbf{1})$  within time  $\tau$ . Note that due to the linearity of the forward SDE, convergence is exponentially fast [45].

The backward SDE that reverses  $p_t$  is given by [46]

$$d\mathbf{x} = (2k_B T \nabla_{\mathbf{x}} \log p_t(\mathbf{x}) + \mathbf{x}) dt + \sqrt{2k_B T} d\mathbf{w}, \quad t \in [0, \tau], \quad \mathbf{x}(0) \sim \mathcal{N}(0, k_B T \mathbf{1}), \quad (2)$$

where  $\nabla_{\mathbf{x}} \log p_t(\mathbf{x})$  is referred to as the “score”. Running this SDE from  $t = 0$  to  $t = \tau$  generates a sample from the target distribution. Since  $p_t$  is not known, the learning problem becomes that of approximating the score  $\nabla_{\mathbf{x}} \log p_t(\mathbf{x})$  using the dataset  $\mathcal{D}$ . Approximating the score, rather than the distribution itself, eliminates

\* cb7454@princeton.edu

the need to estimate the normalization constant—which is equivalent to running the system to equilibrium and is typically intractable for complex, high-dimensional distributions. Typically, artificial neural networks are used to approximate the score [35]. Because the score enters the SDE as a driving term, it can be parameterized in terms of physical forces when the coordinates are interpreted as displacements. Here, we parameterize the score using the gradient of the energy in a network of conservative, nonlinear, overdamped oscillators.

We assume that the associated energy can be described by a low-order polynomial, both for the local energy,  $E^l$ , and the coupling energy,  $E^c$ . These energies are parameterized by time-dependent parameters,  $\theta_l = \theta_l(t)$  and  $\theta_c = \theta_c(t)$ . Concretely, the local energy is given by

$$\begin{aligned} E_{\theta_l(t)}^l(\mathbf{x}) \\ := \sum_{n=1}^N \left[ \frac{1}{2} \alpha_n(t) x_n^2 + \frac{1}{4} \beta_n(t) x_n^4 + \frac{1}{6} \gamma_n(t) x_n^6 + f_n^{ext}(t) x_n \right], \end{aligned} \quad (3)$$

where we ensure that  $\gamma_n(t) > 0$  for all  $n$  so that the energy is coercive, and where  $\{f_n^{ext}\}_{n=1}^N$  are external forces. The coupling energy of a pair of coupled oscillators is

$$\begin{aligned} E_{\theta_{nm}(t)}^{\text{pair}}(x_n, x_m) := \frac{1}{2} \kappa_{nm}(t) (x_n - x_m)^2 \\ + \frac{1}{4} \lambda_{nm}(t) (x_n - x_m)^4 + \chi_{nm}(t) x_n x_m^2 + \hat{\chi}_{nm}(t) x_n^2 x_m, \end{aligned} \quad (4)$$

where  $\kappa$  and  $\lambda$  are symmetric linear and quartic couplings, and  $\chi$  and  $\hat{\chi}$  are asymmetric couplings that arise, e.g., in optomechanical [47], magnetic interactions [48] or geometric nonlinearities [49]. The total coupling energy is then given by

$$E_{\theta_c(t)}^c(\mathbf{x}) := \sum_{n=1}^N \sum_{m>n}^N E_{\theta_{nm}(t)}^{\text{pair}}(x_n, x_m). \quad (5)$$

We define the sum of the local and coupling energy as  $\widehat{E}_{\theta(t)} := E^l + E^c$  where  $\theta = \{\theta_l, \theta_c\}$ . The stochastic dynamics considered here are governed by an overdamped Langevin equation:

$$d\mathbf{x} = -\nabla_{\mathbf{x}} E_{\theta(t)}(\mathbf{x}) dt + \sqrt{2k_B T} d\mathbf{w}, \quad (6)$$

where

$$E_{\theta(t)} = 2\widehat{E}_{\theta(t)} - \sum_n x_n^2/2. \quad (7)$$

Comparing Eqs. (6)-(7) to Eq. (2), we tune the parameters such that  $-\nabla_{\mathbf{x}} \widehat{E}_{\theta(t)}/k_B T \approx \nabla_{\mathbf{x}} \log p_t$  and at inference time the total force applied is  $-\nabla_{\mathbf{x}} E_{\theta(t)}(\mathbf{x}) = -2\nabla_{\mathbf{x}} \widehat{E}_{\theta(t)} + \mathbf{x}$ . If the score approximation is sufficiently accurate, then evolving Eq. (6) for time  $\tau$  will yield

a sample from the target distribution, i.e.,  $\mathbf{x}(\tau) \sim p$ . To ensure that  $\mathbf{x}(0) \sim \mathcal{N}(0, k_B T \mathbf{1})$ , the system must reach equilibrium before the reverse integration can begin. This means the system must relax under the force  $-\nabla_{\mathbf{x}} E_{\theta(\tau)}(\mathbf{x}) = -2\nabla_{\mathbf{x}} \widehat{E}_{\theta(\tau)} + \mathbf{x} \approx -\mathbf{x}$ . However, as noted earlier for the forward process, the system relaxes exponentially fast since the target distribution is a simple Gaussian [45]. The inference process thus involves starting from the equilibrium distribution at  $\theta(\tau)$ , and then evolving the system under the reverse drive protocol  $\theta(\tau - t)$ .

*Local learning rule for SM*— We now tackle the learning problem. The SM objective reads [33]

$$\begin{aligned} J_{\text{SM}}(\theta(t)) = \mathbb{E}_{\mathbf{x}_t \sim p_t(\mathbf{x})} \left\{ -\text{Tr} \nabla_{\mathbf{x}}^2 \widehat{E}_{\theta(t)}(\mathbf{x}_t) / (k_B T) \right. \\ \left. + \frac{1}{2} \|\nabla_{\mathbf{x}} \widehat{E}_{\theta(t)}(\mathbf{x}_t)\|^2 / (k_B T)^2 \right\}. \end{aligned} \quad (8)$$

The force matching update rule is then obtained by computing the gradient of the objective with respect to the  $i$ -th parameter:

$$\begin{aligned} \frac{dJ_{\text{SM}}}{d\theta_i(t)} = \mathbb{E}_{\mathbf{x}_t \sim p_t(\mathbf{x})} \left\{ -\text{Tr} \nabla_{\mathbf{x}}^2 \frac{d\widehat{E}_{\theta(t)}}{d\theta_i(t)} / (k_B T) \right. \\ \left. + \sum_n \left[ \nabla_{\mathbf{x}} \frac{d\widehat{E}_{\theta(t)}}{d\theta_i(t)} \right]_n \left[ \nabla_{\mathbf{x}} \widehat{E}_{\theta(t)} \right]_n / (k_B T)^2 \right\}, \end{aligned} \quad (9)$$

where we used that the parameter and state derivatives can be exchanged by construction of the energy.

Because any parameter  $\theta_i(t)$  enters the energy linearly,  $d\widehat{E}_{\theta(t)}/d\theta_i(t)$  is independent of the parameters and can—just as its  $x$ -derivatives—be evaluated trivially. Finally,  $\nabla_{\mathbf{x}} \widehat{E}_{\theta(t)}$  can be identified as the negative force, i.e.  $-\widehat{\mathbf{f}}_{\theta(t)} := \nabla_{\mathbf{x}} \widehat{E}_{\theta(t)} = (\nabla_{\mathbf{x}} E_{\theta(t)} + \mathbf{x})/2$ . It can be obtained by clamping the network to the sample  $\mathbf{x}_t$  and measuring the force acting on each oscillator  $\mathbf{f}_{\theta(t)} = -\nabla_{\mathbf{x}} E_{\theta(t)}$ , hence the name “force matching”. Alternatively, if the negative quadratic potential  $\sum_n x_n^2/2$  and the factor 2 in Eq. (7) can be turned off during training,  $\widehat{\mathbf{f}}_{\theta(t)}$  can be measured directly.

To train the system, we perform the standard approximation of  $p \approx p_{t=0}^{\mathcal{D}} := \sum_{m=1}^M \delta(\mathbf{x} - \mathbf{x}^{(m)})/M$  [34]. For the forward process in Eq. (1), this yields an approximate probability flow  $p_t^{\mathcal{D}} \approx p_t$ , where  $p_t^{\mathcal{D}}$  is a mixture of Gaussians from which we can easily draw samples [34, 36]. We denote the  $m$ -th sample from  $p_t^{\mathcal{D}}$  as  $\mathbf{x}_t^{(m)}$ . We discretize time into  $N_t$  time points,  $t_0 = 0, \dots, t_{N_t-1} = \tau$ , and solve the minimization of  $J_{\text{SM}}$  sequentially. To ensure smoothness in the parameter evolution, the learning problem at time  $t_{n+1}$  is initialized using the parameters learned at time  $t_n$ . The resulting set of learned parameters,  $\{\theta^*(0), \dots, \theta^*(N_t-1)\}$ , is then interpolated and applied as the driving protocol at inference time. The rate of change in the parameters can be controlled via the temperature: lower temperatures lead to smoother

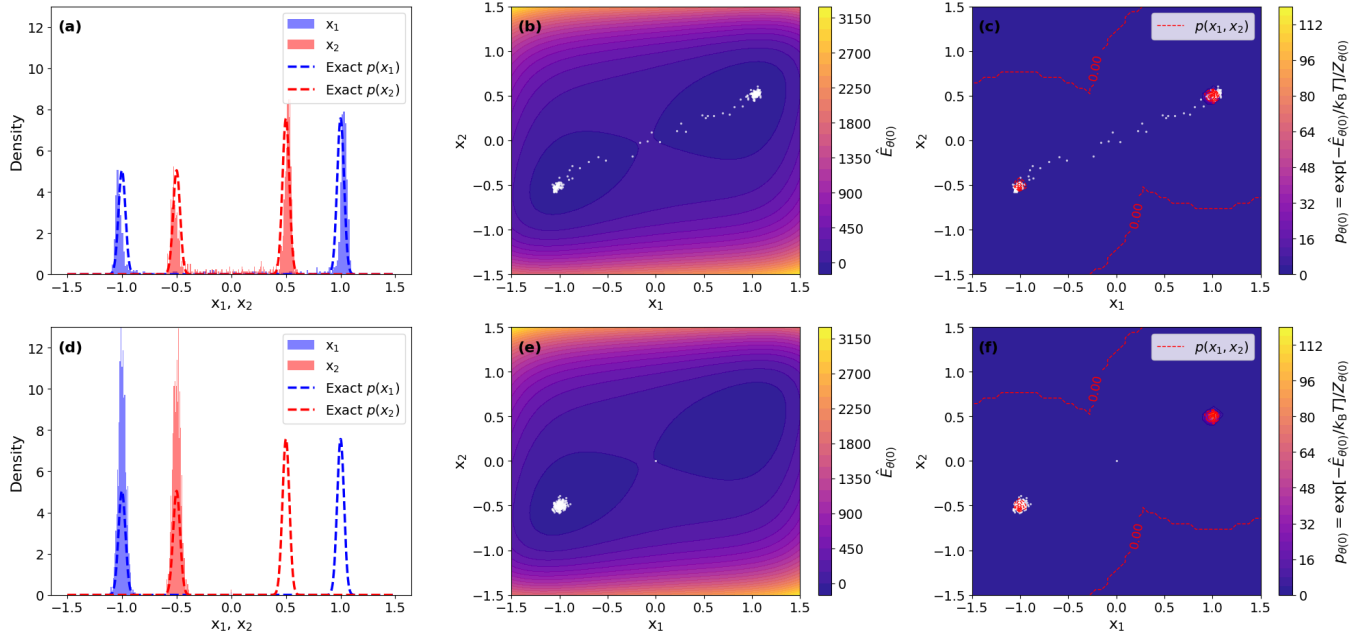


FIG. 1. (a) 1000 samples drawn via the learned reverse-time SDE from a 2-oscillator network overlaid with the exact marginals of  $p(x_1, x_2)$ . (b) Learned energy landscape  $\hat{E}_{\theta(0)}$  at  $t = 0$  (beginning of the forward, final time of the reverse process), with reverse-time SDE samples. (c) Iso-contours of  $p(x_1, x_2)$  (red) overlaid on the Boltzmann distribution,  $p_{\theta(0)}(x_1, x_2) = \exp[-\hat{E}_{\theta(0)}(x_1, x_2)/k_B T]/Z_{\theta(0)}$ , of the learned energy.  $Z_{\theta(0)}$  is the partition function. (d)–(f) Corresponding results for ES.

parameter evolution. As an example, consider the Duffing parameter of the  $n$ -th oscillator,  $\beta_n$ , at time  $t_l$  and we draw  $M$  samples from  $p_t^{\mathcal{D}}$ :

$$\frac{dJ_{\text{SM}}}{d\beta_n(t_l)} = \sum_{m=1}^M \frac{1}{M} \left\{ -3(x_n^{(m)})^2/(k_B T) - (x_n^{(m)})^3 \hat{f}_{n,\theta(t_l)}(\mathbf{x}^{(m)})/(k_B T)^2 \right\}. \quad (10)$$

In case force measurements are not accessible, the SM objective gradient can instead be obtained from contrastive divergence with one time step (CD1) [50]. The CD1 loss function is given by

$$J_{\text{CD1}}(\theta(t)) = \mathbb{E}_{\mathbf{x}_t \sim p_t(\mathbf{x}), \mathbf{w} \sim \mathcal{N}(0, \mathbb{1})} \left\{ -\hat{E}_{\theta(t)}(\mathbf{x}_t) + \hat{E}_{\theta(t)}(\mathbf{x}_{t+\delta}) \right\}. \quad (11)$$

The network state evolved by infinitesimal time increment,  $\mathbf{x}_{t+\delta}$ , can be obtained physically if the quadratic potential and the factor 2 in Eq. (7) can be turned off during training. Then the network with energy  $\hat{E}_{\theta(t)}$  can be initialized at  $\mathbf{x}_t$  and letting it evolve for time  $\delta$  will allow us to measure  $\mathbf{x}_{t+\delta}$ . In practice the evolution time,  $\delta$ , must be small compared to the fastest internal time scale. This must be repeated multiple times to estimate the expectation over noise. Formally, we have

$$\mathbf{x}_{t+\delta} = \mathbf{x}_t - \nabla_{\mathbf{x}} \hat{E}_{\theta(t)}(\mathbf{x}_t) \delta + \sqrt{2\delta k_B T} \mathbf{w}, \quad (12)$$

where  $\mathbf{w} \sim \mathcal{N}(0, \mathbb{1})$ .

In Hyvärinen [50] the correspondence between CD1 and SM was derived for a unit noise strength, which can naturally be extended to finite temperature. In the limit where  $\delta \rightarrow 0$  we find

$$\frac{dJ_{\text{SM}}}{d\theta_i(t)} = -\frac{1}{\delta(k_B T)^2} \frac{dJ_{\text{CD1}}}{d\theta_i(t)}. \quad (13)$$

As in the previous case, since the network parameters enter the energy linearly the derivative  $dJ_{\text{CD1}}/d\theta$  reduces to a difference of polynomials in the states evaluated at times  $t$  and  $t + \delta$ . For the  $n$ -th Duffing parameter at time  $t_l$  we obtain

$$\frac{dJ_{\text{CD1}}}{d\beta_n(t_l)} = \sum_{m=1}^M \frac{1}{4M} \mathbb{E}_{\mathbf{w} \sim \mathcal{N}(0, \mathbb{1})} \left\{ -(x_{n,t_l}^{(m)})^4 + (x_{n,t_l+\delta}^{(m)})^4 \right\}. \quad (14)$$

Hence, to compute the gradient at each time step  $t_l$ , the system is initialized multiple times at the same data point  $\mathbf{x}_{t_l}^{(m)}$  and evolved for a duration  $\delta$  under different noise realizations. And since the network parameters do not appear in the gradient expression explicitly, no knowledge of the parameter values is required.

*Sampling from a mixture of Gaussians and MNIST*—We first apply the presented framework to sample from a mixture of two Gaussians in 2D, i.e.,  $p(x_1, x_2) = \omega_1 \mathcal{N}(x_1, x_2 | \boldsymbol{\mu}_1, \boldsymbol{\Sigma}_1) + \omega_2 \mathcal{N}(x_1, x_2 | \boldsymbol{\mu}_2, \boldsymbol{\Sigma}_2)$ . Iso-contours are shown in Fig. 1(c) and (d) in red, and its marginals,  $p(x_1)$  and  $p(x_2)$ , are plotted as dashed red and blue lines, respectively, in Fig. 1(a) and (d).

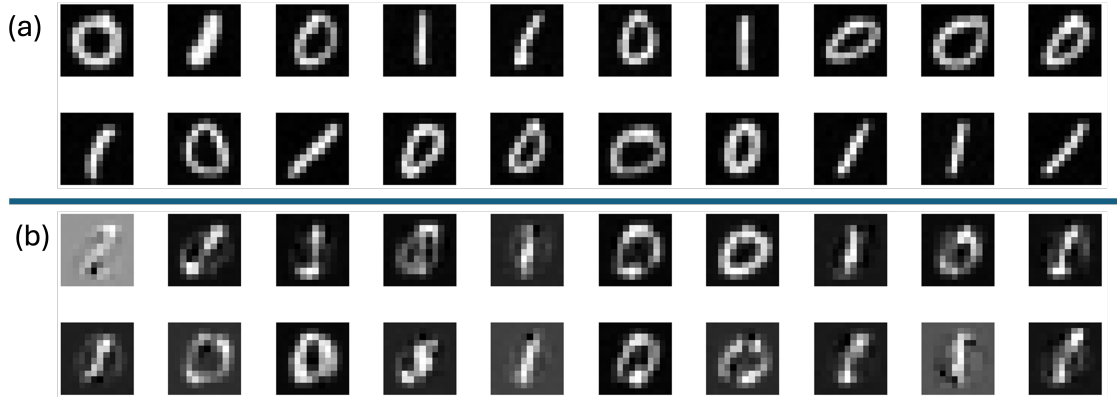


FIG. 2. (a) Examples of “0”s and “1”s from the MNIST dataset down-sampled to  $12 \times 12$  pixels. (b) Samples generated with the network of  $12 \times 12$  nonlinear, overdamped oscillators.

To demonstrate the advantages of out-of-equilibrium sampling even in this low-dimensional setting, we compare the samples it produces (first row of Fig. 1) with those obtained by ES (second row of Fig. 1). We use the force matching learning rule in Eq. (9) to train a 2-oscillator network. Details on the training are provided in the Supplemental Material. Training yields  $\hat{E}_{\theta(t)}(x_1, x_2)$ . For the SGM we run Eq. (6) with  $-\nabla_{\mathbf{x}} E_{\theta(t)}(\mathbf{x}) = -2\nabla_{\mathbf{x}} \hat{E}_{\theta(t)} + \mathbf{x}$  for  $t \in [0, \tau]$ . We repeat this procedure  $S = 1000$  times to generate 1000 samples. For ES we run the static SDE with force  $-\nabla_{\mathbf{x}} \hat{E}_{\theta(0)}$  for a time of  $\tau \times S$ . One can observe that ES becomes trapped in the high-probability region on the left, while SGM manages to recover samples from both modes with approximately the correct weights.

In the Supplemental Material, we also train an oscillator network using the CD1 learning rule to generate samples from a mixture of Gaussians. We observe that CD1 can lead to spurious high-probability modes in the learned energy landscape, which may affect sample quality. In contrast, force matching (Eq. (9)) yields a more faithful and robust approximation and is therefore preferred for larger-scale problems. Although CD1 can still produce high-quality samples in simple settings, force matching proved more reliable overall. We therefore apply force matching to the larger task of training an oscillator network on the MNIST dataset to generate images of handwritten digits “0” and “1”. The images are down-sampled to  $12 \times 12$  pixels, corresponding to a network of  $12 \times 12$  coupled oscillators. Fig. 2 (a) shows representative training images, and Fig. 2 (b) displays novel samples generated by the trained oscillator network. The images were generated using long-range couplings between oscillators up to 6 sites apart. In the Supplemental Material, we study how reducing the number of long-range couplings affects image quality. We find that the quality degrades only gradually down to 3 long-range couplings, below which it deteriorates significantly.

*Conclusions and outlook*— In this work, we have

shown that diffusion models, an out-of-equilibrium system, can be trained with local learning rules. In particular, we introduced force matching that allows us to train SGMs on a network of nonlinear, overdamped oscillators coupled to a thermal bath. Parameter gradients are obtained directly from force measurements. Numerically, we demonstrate that the force matching approach can (i) sample from a mixture of two Gaussians in 2D, and (ii) scale up to a  $12 \times 12$  oscillator network that successfully samples binarized “0”s and “1”s from MNIST. Alternatively, we showed that CD1 can be harnessed and the updates can be computed from repeated one-step observations of the physical dynamics.

Future research should study the trade-offs between network size, coupling topology, and sampling performance. Furthermore, exploring latent-space SGMs [51] to identify more natural embeddings for the physical system at hand is expected to increase expressivity. Interestingly, it has recently been shown that locality in the score function can give rise to creativity [52], suggesting that what may appear to be a major constraint in physical systems—locality—could in fact be beneficial for generative models. Hence, our results may inspire novel forms of unconventional computing for generative modeling.

*Acknowledgments*— We thank Cindy Zhang for helpful discussions. C.B. was supported by the Swiss National Science Foundation (SNSF) through a Postdoc.Mobility fellowship (P500PT 217673/1). This work was performed in part at Aspen Center for Physics, which is supported by National Science Foundation grant PHY-2210452. M.G. was funded by the European Union. Views and opinions expressed are however those of the author(s) only and do not necessarily reflect those of the European Union or the European Research Council Executive Agency. Neither the European Union nor the granting authority can be held responsible for them. This work is supported by the ERC grant 101040117 (INFOPASS) and NSF OAC-2118201.

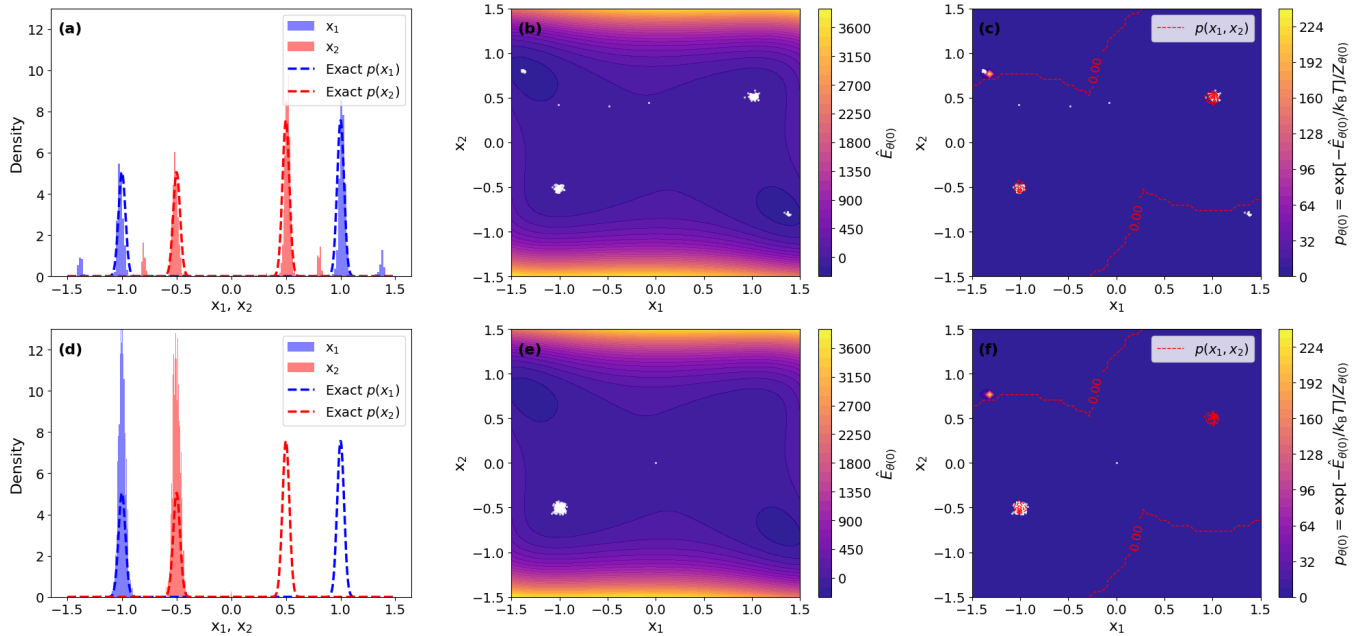


FIG. 3. Training via CD1 learning rule: (a) 1000 samples drawn via the learned reverse-time SDE from a 2-oscillator network overlaid with the exact marginals of  $p(x_1, x_2)$ . (b) Learned energy landscape  $\hat{E}_{\theta(0)}$  at  $t = 0$  (beginning of the forward, final time of the reverse process), with reverse-time SDE samples. (c) Iso-contours of  $p(x_1, x_2)$  (red) overlaid on the Boltzmann distribution,  $p_{\theta(0)}(x_1, x_2) = \exp[-\hat{E}_{\theta(0)}(x_1, x_2)/k_B T]/Z_{\theta(0)}$ , of the learned energy.  $Z_{\theta(0)}$  is the partition function. (d)–(f) Corresponding results for ES.

### Appendix A: Training

For the examples shown, we initialized the learning problems as follows: for all  $n$ , we set  $\alpha_n = -1$ ,  $\beta_n = 1$ , and  $\gamma_n = 1$ . All other parameters, including external forces and couplings, were initialized to zero. Furthermore, we set the temperature to  $k_B T = 0.005$ . During optimization, we enforce  $\gamma_n > 0.001$  to ensure that the energy remains bounded from below and grows at large  $|x|$ , guaranteeing a physically well-defined potential. At this temperature, the forward process converges with sufficient accuracy to  $p_\tau \approx \mathcal{N}(0, k_B T \mathbf{1})$  within a time of  $\tau = 4$ . We then solve the optimization sequentially for  $t_0 = 0, \dots, t_{N_t-1} = \tau$ , where  $N_t = 15$ . All training and simulations were performed on a single NVIDIA L40 GPU.

### Appendix B: CD1 example

Figure 3 shows an example of a 2-oscillator network trained using the CD1 learning rule (see Eq. (11)). The resulting energy landscape differs from the one obtained with force matching and exhibits spurious high-probability modes. Despite these artifacts, only a few samples are drawn from these spurious modes, and most non-equilibrium samples remain of high quality. This suggests that during the out-of-equilibrium evolution, samples are steered toward the correct modes, even if

those modes are assigned lower probability by the learned energy landscape at  $t = 0$ .

### Appendix C: Number of long-range couplings

We investigate the effect of long-range couplings on the quality of generated images (Fig. 4). To this end, we progressively reduce the number of long-range couplings from 6 (Fig. 4a) to 1 (Fig. 4f). While the expressive power of the system initially declines slowly, it deteriorates significantly when fewer than 3 long-range couplings remain.

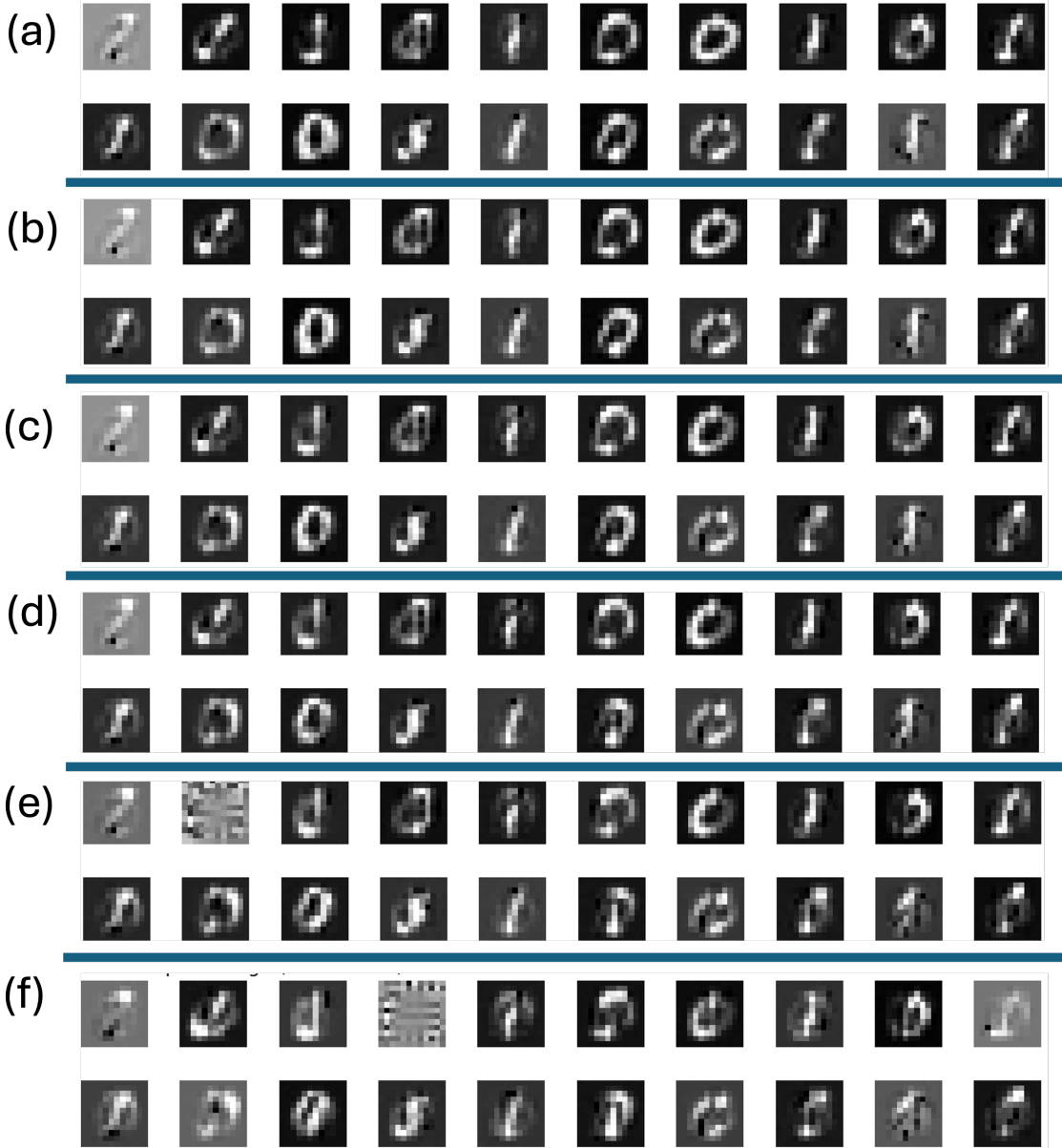


FIG. 4. Influence of number of couplings on  $12 \times 12$  MNIST image generation: 6 (a), 5 (b), 4 (c), 3 (d), 2 (e) and 1 (f) long-range couplings.

---

[1] H. Jaeger, B. Noheda, and W. G. Van Der Wiel, Toward a formal theory for computing machines made out of whatever physics offers, *Nature communications* **14**, 4911 (2023).

[2] R. Yanagimoto, B. A. Ash, M. M. Sohoni, M. M. Stein, Y. Zhao, F. Presutti, M. Jankowski, L. G. Wright, T. Onodera, and P. L. McMahon, Programmable on-chip nonlinear photonics, *arXiv:2503.19861* (2025).

[3] G. Finocchio, J. A. C. Incovia, J. S. Friedman, Q. Yang, A. Giordano, J. Grollier, H. Yang, F. Ciubotaru, A. V. Chumak, A. J. Naeemi, *et al.*, Roadmap for unconventional computing with nanotechnology, *Nano Futures* **8**, 012001 (2024).

[4] D. Melanson, M. Abu Khater, M. Aifer, K. Donatella, M. Hunter Gordon, T. Ahle, G. Crooks, A. J. Martinez, F. Sbahi, and P. J. Coles, Thermodynamic computing system for ai applications, *Nature Communications* **16**, 3757 (2025).

[5] M. Aifer, K. Donatella, M. H. Gordon, S. Duffield, T. Ahle, D. Simpson, G. Crooks, and P. J. Coles, Thermodynamic linear algebra, *npj Unconventional Computing* **1**, 13 (2024).

[6] S. Duffield, M. Aifer, G. Crooks, T. Ahle, and P. J. Coles, Thermodynamic matrix exponentials and thermo-

dynamic parallelism, *Physical Review Research* **7**, 013147 (2025).

[7] P. Lipka-Bartosik, K. Donatella, M. Aifer, D. Melanson, M. Perarnau-Llobet, N. Brunner, and P. J. Coles, Thermodynamic algorithms for quadratic programming, in *2024 IEEE International Conference on Rebooting Computing (ICRC)* (IEEE, 2024) pp. 1–13.

[8] M. Anderson, S.-Y. Ma, T. Wang, L. Wright, and P. McMahon, Optical transformers, *Transactions on Machine Learning Research* (2023).

[9] M. Yildirim, N. U. Dinc, I. Oguz, D. Psaltis, and C. Moser, Nonlinear processing with linear optics, *Nature Photonics* **18**, 1076 (2024).

[10] C. C. Wanjura and F. Marquardt, Fully nonlinear neuromorphic computing with linear wave scattering, *Nature Physics* **20**, 1434 (2024).

[11] N. Richardson, C. Bösch, and R. P. Adams, Nonlinear computation with linear optics via source-position encoding, *arXiv:2504.20401* (2025).

[12] J. Lin, F. Barrows, and F. Caravelli, Memristive linear algebra, *Physical Review Research* **7**, 023241 (2025).

[13] K. Nakajima, H. Hauser, T. Li, and R. Pfeifer, Information processing via physical soft body, *Scientific reports* **5**, 10487 (2015).

[14] I. Oguz, N. Dinc, M. Yildirim, J. Ke, I. Yoo, Q. Wang, F. Yang, C. Moser, and D. Psaltis, Optical diffusion models for image generation, *Advances in Neural Information Processing Systems* **37**, 59150 (2024).

[15] D. Hebb, *The organization of behavior* (1949).

[16] J. J. Hopfield, Neural networks and physical systems with emergent collective computational abilities., *Proceedings of the national academy of sciences* **79**, 2554 (1982).

[17] Y. Bengio, D.-H. Lee, J. Bornschein, T. Mesnard, and Z. Lin, Towards biologically plausible deep learning, *arXiv:1502.04156* (2015).

[18] M. Stern and A. Murugan, Learning without neurons in physical systems, *Annual Review of Condensed Matter Physics* **14**, 417 (2023).

[19] B. Scellier and Y. Bengio, Equilibrium propagation: Bridging the gap between energy-based models and back-propagation, *Frontiers in computational neuroscience* **11**, 24 (2017).

[20] V. R. Anisetti, A. Kandala, B. Scellier, and J. Schwarz, Frequency propagation: Multimechanism learning in nonlinear physical networks, *Neural Computation* **36**, 596 (2024).

[21] M. Stern, D. Hexner, J. W. Rocks, and A. J. Liu, Supervised learning in physical networks: From machine learning to learning machines, *Physical Review X* **11**, 021045 (2021).

[22] V. Lopez-Pastor and F. Marquardt, Self-learning machines based on hamiltonian echo backpropagation, *Physical Review X* **13**, 031020 (2023).

[23] D. de Bos and M. Serra-Garcia, Learning in a multifield coherent ising machine, *arXiv:2502.12020* (2025).

[24] S. Dillavou, M. Stern, A. J. Liu, and D. J. Durian, Demonstration of decentralized physics-driven learning, *Physical Review Applied* **18**, 014040 (2022).

[25] S. Dillavou, B. D. Beyer, M. Stern, A. J. Liu, M. Z. Miskin, and D. J. Durian, Machine learning without a processor: Emergent learning in a nonlinear analog network, *Proceedings of the National Academy of Sciences* **121**, e2319718121 (2024).

[26] J. Laydevant, D. Marković, and J. Grollier, Training an ising machine with equilibrium propagation, *Nature Communications* **15**, 3671 (2024).

[27] S. Niazi, S. Chowdhury, N. A. Aadit, M. Mohseni, Y. Qin, and K. Y. Camsari, Training deep boltzmann networks with sparse ising machines, *Nature Electronics* **7**, 610 (2024).

[28] M. Ernoult, J. Grollier, and D. Querlioz, Using memristors for robust local learning of hardware restricted boltzmann machines, *Scientific reports* **9**, 1851 (2019).

[29] J. Kaiser, W. A. Borders, K. Y. Camsari, S. Fukami, H. Ohno, and S. Datta, Hardware-aware in situ learning based on stochastic magnetic tunnel junctions, *Physical Review Applied* **17**, 014016 (2022).

[30] N. S. Singh, K. Kobayashi, Q. Cao, K. Selcuk, T. Hu, S. Niazi, N. A. Aadit, S. Kanai, H. Ohno, S. Fukami, *et al.*, Cmos plus stochastic nanomagnets enabling heterogeneous computers for probabilistic inference and learning, *Nature Communications* **15**, 2685 (2024).

[31] Q. Wang, C. C. Wanjura, and F. Marquardt, Training coupled phase oscillators as a neuromorphic platform using equilibrium propagation, *Neuromorphic Computing and Engineering* **4**, 034014 (2024).

[32] P. Baldi and F. Pineda, Contrastive learning and neural oscillations, *Neural computation* **3**, 526 (1991).

[33] A. Hyvärinen, Estimation of non-normalized statistical models by score matching, *Journal of Machine Learning Research* **6**, 695 (2005).

[34] Y. Song and S. Ermon, Generative modeling by estimating gradients of the data distribution, *Advances in neural information processing systems* **32** (2019).

[35] Y. Song, J. Sohl-Dickstein, D. P. Kingma, A. Kumar, S. Ermon, and B. Poole, Score-based generative modeling through stochastic differential equations, *arXiv:2011.13456* (2021).

[36] T. Dockhorn, A. Vahdat, and K. Kreis, Score-based generative modeling with critically-damped langevin diffusion, *arXiv:2112.07068* (2021).

[37] C. Saharia, W. Chan, S. Saxena, L. Li, J. Whang, E. L. Denton, K. Ghasemipour, R. Gontijo Lopes, B. Karagol Ayan, T. Salimans, *et al.*, Photorealistic text-to-image diffusion models with deep language understanding, *Advances in neural information processing systems* **35**, 36479 (2022).

[38] J. S. Lee, J. Kim, and P. M. Kim, Score-based generative modeling for de novo protein design, *Nature Computational Science* **3**, 382 (2023).

[39] G. E. Hinton, T. J. Sejnowski, *et al.*, Learning and re-learning in boltzmann machines, *Parallel distributed processing: Explorations in the microstructure of cognition* **1**, 2 (1986).

[40] G. E. Hinton, Training products of experts by minimizing contrastive divergence, *Neural computation* **14**, 1771 (2002).

[41] R. Salakhutdinov and H. Larochelle, Efficient learning of deep boltzmann machines, in *Proceedings of the thirteenth international conference on artificial intelligence and statistics* (JMLR Workshop and Conference Proceedings, 2010) pp. 693–700.

[42] R. M. Neal, Probabilistic inference using markov chain monte carlo methods, Technical Report CRG-TR-93-1, Department of Computer Science, University of Toronto (1993).

[43] Y. Lipman, R. T. Chen, H. Ben-Hamu, M. Nickel, and M. Le, Flow matching for generative modeling, arXiv:2210.02747 (2022).

[44] J. Ho, A. Jain, and P. Abbeel, Denoising diffusion probabilistic models, *Advances in neural information processing systems* **33**, 6840 (2020).

[45] S. Vempala and A. Wibisono, Rapid convergence of the unadjusted langevin algorithm: Isoperimetry suffices, *Advances in neural information processing systems* **32** (2019).

[46] B. D. Anderson, Reverse-time diffusion equation models, *Stochastic Processes and their Applications* **12**, 313 (1982).

[47] J. C. Sankey, C. Yang, B. M. Zwickl, A. M. Jayich, and J. G. Harris, Strong and tunable nonlinear optomechanical coupling in a low-loss system, *Nature Physics* **6**, 707 (2010).

[48] M. Serra-Garcia, M. Molerón, and C. Daraio, Tunable, synchronized frequency down-conversion in magnetic lattices with defects, *Philosophical Transactions of the Royal Society A: Mathematical, Physical and Engineering Sciences* **376**, 20170137 (2018).

[49] M. Serra-Garcia, A. Foehr, M. Molerón, J. Lydon, C. Chong, and C. Daraio, Mechanical autonomous stochastic heat engine, *Physical review letters* **117**, 010602 (2016).

[50] A. Hyvarinen, Connections between score matching, contrastive divergence, and pseudolikelihood for continuous-valued variables, *IEEE Transactions on neural networks* **18**, 1529 (2007).

[51] A. Vahdat, K. Kreis, and J. Kautz, Score-based generative modeling in latent space, *Advances in neural information processing systems* **34**, 11287 (2021).

[52] M. Kamb and S. Ganguli, An analytic theory of creativity in convolutional diffusion models, arXiv:2412.20292 (2024).